

## Testing the Time-predictable Earthquake Recurrence Model

Jessica Murray, Paul Segall

Geophysics Department  
Stanford University  
Stanford, CA 94305-2215

### ABSTRACT

**The time-predictable earthquake recurrence model, incorporated in many seismic hazard predictions, states that an earthquake occurs when the fault recovers the stress relieved in the most recent earthquake. We estimated rigorous bounds on the predicted recurrence time of the  $M \sim 6$  1966 Parkfield, CA earthquake through inversion of geodetic measurements. According to the time predictable model, the earthquake should have occurred by 1987. That the model fails in a relatively simple, well-studied tectonic setting does not bode well for its successful application in complex regions like the San Francisco Bay area or Southern California.**

Probabilistic hazard estimates use various models for the temporal distribution of earthquakes (1). One that is widely cited is the time-predictable model (2), in which the time to the next earthquake is the stress drop in the most recent earthquake divided by the fault stressing-rate. Although stress is difficult to measure in situ, the earth's crust is linearly elastic, so strain is a valid proxy for stress.

There are several reasons to believe that earthquake occurrence should not be well described by a simple point model such as this. Earthquakes rupture finite areas, so the time-predictable model must be applied to a well-defined fault segment. Fault "segmentation", however, has proven difficult to apply in many places (e.g. Landers, 3). Conditions for unstable

slip may be met locally on the fault; how large the earthquake eventually becomes depends on complex rupture dynamics. Furthermore, the rate of stress accumulation on the fault may be non-steady, either due to local creep processes or external sources such as nearby earthquakes. The time-predictable model posits the existence of a fixed threshold stress. However, modern theories of slip instability show that earthquake nucleation results from an interaction of the slip surface with the elastic surroundings such that earthquakes need not occur at a fixed failure stress (4, 5). This motivates us to test the validity of the model in a simple, well-understood seismo-tectonic setting.

The Parkfield segment of the San Andreas fault (Fig. 1A) forms a transition between the creeping segment to the northwest and the locked section that last ruptured in the  $M$  8 1857 Fort Tejon earthquake to the southeast. At least 5 historic earthquakes of  $M \sim 6$ , have occurred in this area, most recently in 1966. These events, which are similar in character, have an average recurrence time of 22 years (6). Bakun and McEvilly (7) predicted the next earthquake there would occur in  $1988 \pm 5$  years. Geodetic measurements have been made for over 35 years at Parkfield (8-10), making it one of the few places where geodetic strain has been measured for times exceeding the average inter-event time. The similarity among these events, along with the simple fault geometry consisting of a single strand of the San Andreas fault, suggests that if the time-predictable model were to work anywhere, it should work here.

Inversion of geodetic data collected since 1966 has shown that although the San Andreas exhibits shallow creep near Parkfield, the fault is either locked or slowly slipping at depth (e.g., Fig 1B, 10-12). This demonstrates that strain has been accumulating throughout what has now become the longest recorded interseismic period for  $M \sim 6$  earthquakes at Parkfield. If we can

show with a high degree of confidence that the strain released in 1966 has already accumulated, then the time-predictable model has failed.

We began by approximating the complex loading of the shallow seismogenic zone by aseismic slip at a constant rate on a downward extension of the fault (13). If the seismogenic fault were slipping everywhere at the long-term deep slip-rate, no strain would accumulate. If the slip-rate is spatially variable, however, some parts of the fault will experience a slip-deficit in comparison to the long-term slip. This allows one to express the predicted interevent time as the ratio of the coseismic moment release to the interseismic moment deficit rate (14, 15).

The geodetic data (16) can be used to estimate the slip distribution for the 1966 earthquake and the slip-rate distribution for the interseismic period (1966 to 1998), from which the coseismic moment ( $M_o$ ) and interseismic moment deficit rate ( $\dot{M}_d$ ) can be derived. We adopted a model fault geometry that is consistent with the surface fault trace and microseismicity (Fig. 1). This model includes a transition depth below which the fault was assumed to slip aseismically at the long-term deep slip-rate. There is a well known tradeoff between the estimated transition depth and deep slip-rate; the greater the transition depth the higher the deep slip-rate (10, 11). Inversion of geodetic data for fault slip is nonunique. Rather than seek a particular estimate by regularizing the inversion (e.g., imposing spatial smoothing), we followed Johnson et al. (17) and determined rigorous bounds on  $M_o$  and  $\dot{M}_d$ . These bounds are not contingent on a regularizing functional. From the ratio of  $M_o$  and  $\dot{M}_d$  we obtained bounds on the predicted interevent time, which allowed us to test the time predictable model.

Using data up to 1984, Segall and Harris (14) found interevent times from 5 to 29 years. Their analysis was restricted to regularized inversions, and they did not develop a probability distribution of recurrence times. In the present study, we analyzed nearly twice as much data

(16) consisting of 1) coseismic line-length changes, 2) interseismic rates of line-length change (1967 – 1991), and 3) GPS velocities (Fig 1A, 1991 – 1998). We employed constrained inversion to determine moments consistent with the data without assumptions implicit in regularized inversions. Bootstrap methods (18, 19) were then used to incorporate uncertainty in the transition depth and deep slip-rate and to determine rigorous bounds on interevent time.

Constrained inversion involves finding the slip distribution that best fits the data, subject to the constraint that the seismic moment equals a specified value. Slip was constrained to be positive (right lateral), but we made no assumption of smoothness (Fig. 2A) (20). We swept through a range of moments and found a best-fitting solution for each one (Fig. 2B). The moment with the lowest misfit is optimal in the sense that there are no slip distributions resulting in different moments that fit the data better. The range of moments that fit the data acceptably well is more important than the best fitting moment. To identify the range of moments consistent with the data, we used the bootstrap, repeating the constrained inversions for best-fitting  $M_0$  4,000 times. We found this method to be successful in empirical tests using synthetic data (Fig. 2C). The same was done for the interseismic period to infer the distribution for  $\dot{M}_d$ .

The resulting estimates of  $M_0$  and  $\dot{M}_d$  are conditional on an assumed transition depth, and in the case of  $\dot{M}_d$ , deep slip-rate. Although the geodetic data provide some constraints on these parameters, they are not uniquely resolved. Murray et al. (10) found from damped least squares inversions with a smoothing parameter chosen by cross validation (21) that the misfit,  $\mathbf{r}^T \Sigma^{-1} \mathbf{r}$ , is a nearly quadratic function of transition depth and deep slip-rate. Noting that for linear least squares the misfit is quadratic, and the corresponding probability density function (pdf) of the parameters is Gaussian and proportional to  $e^{-\mathbf{r}^T \Sigma^{-1} \mathbf{r}}$ , we used the observed misfit distribution to approximate the joint pdf for transition depth and deep slip-rate (Fig. 3). Each time the data

were resampled in the bootstrap, a new transition depth / deep slip-rate pair was chosen from this empirical distribution.

The range of coseismic moments estimated from the bootstrap resamples (Fig. 4A) is consistent with other estimates based on geodetic data (14, 22), corresponding to  $M_w$  between 6.3 and 6.6, but considerably larger than those found using surface waves ( $M_o$  between  $0.9 \times 10^{18}$  and  $2.1 \times 10^{18}$  Nm) (23). There are several explanations for this discrepancy. The trilateration data spanning the earthquake were collected fairly close to the fault and thus are insensitive to deeper slip. The inversions can place significant slip at depth without causing large misfit to the data (Fig. 2A). In addition, considerable afterslip was observed following this event (24). Since we are interested in the time needed to accumulate the total moment associated with this earthquake, it is irrelevant whether the slip occurred during fast rupture or post-seismic transient.

The moment deficit rates estimated from the trilateration and GPS data are comparable, with slightly greater values found using the trilateration data (25) (Fig. 4B,C). The distribution for interevent time was found from the ratios of  $M_o$  to  $\dot{M}_d$  (26) using the same transition depth (Fig. 4D). The resulting bounds on interevent time range from 7 to 21 years at 95% confidence. In other words, the strain released in 1966 recovered sometime between 1973 and 1987.

Why does the time predictable model fail to predict the Parkfield earthquake? A central premise of the time-predictable model, that an earthquake occurs when the fault reaches a critical stress, may be inaccurate. Variations in pore fluid pressure in the nucleation zone could modulate the stress required for an earthquake to nucleate. Moreover, formulations for fault failure such as rate and state friction do not embody a characteristic failure stress. Rather, acceleration toward unstable slip depends on the elastic loading system and the frictional properties of the fault. Stress perturbations may lead to evolution of the fault 'state' and thus

affect the time to the next earthquake (27). For example, the Coalinga earthquake of 1983 may have delayed the next Parkfield earthquake into the mid 1990s, however this does not explain the extended quiescence (28). The  $M \sim 4.7$  Parkfield events in the early 1990s almost certainly increased the static stress in the expected nucleation zone, increasing the probability of a repeat of the 1966 event (29).

There may also be a much longer scale decrease in stressing rate following the 1857 Fort Tejon earthquake, which has led to the suggestion that the recurrence times of Parkfield earthquakes should increase with time (30). However, the fact that the recent GPS data predict a deep slip-rate consistent with the geologic rate (10) suggests that transient effects due to the 1857 event may be small. Furthermore, in this study we used actual measurements of strain accumulation rather than assuming a constant loading rate.

That the time-predictable model fails at Parkfield is an indication that there are crucial aspects of earthquake physics, even in a fairly simple and well understood setting, that this model does not capture. Although the time-predictable model may approximate the long-term average behavior of some faults, it does not appear to produce useful results for hazard predictions on short to medium time scales.

Another recurrence model is the slip-predictable model (2) which posits that the slip in the next earthquake equals the accumulated slip deficit. This model cannot be tested until the next Parkfield quake. However given the current slip deficit rate, were the earthquake to occur in 2002 the slip predictable model would require a moment of  $9.2 \times 10^{18}$  Nm to  $2.6 \times 10^{19}$  Nm ( $M_w = 6.6 - 6.9$ ), considerably larger than the 1966 earthquake.

## Figure Captions

**Figure 1:** (A) The San Andreas Fault in the Parkfield area (town of Parkfield indicated by star). Blue vectors indicate velocities of GPS stations (1991 – 1998). Model fault trace based on geology and seismicity (*10*), is shown as black and red line; the red portion is the seismogenic fault which is divided into subfaults (dislocations). (B) Slip estimated for each subfault after (*10*). For the interseismic period we simulate the creeping section to the northwest and the steadily slipping fault below the transition depth with uniformly slipping dislocations (note that these dislocations are larger than shown in (B)). The slip-deficit rate is defined as the difference between the deep slip-rate and the slip rate on the seismogenic fault.

**Figure 2:** (A) Slip distributions from constrained inversion corresponding to (top) the minimum ( $3.2 \times 10^{18}$  Nm) and (bottom) the maximum ( $7.9 \times 10^{18}$  Nm) coseismic moment (95% confidence) assuming a transition depth of 14 km. For the minimum moment the inversion has placed the slip at the southeastern end of the fault where the geodetic measurements were concentrated. For the maximum moment, significant slip is placed at depth and at the northwestern end where the data resolution is poor. (B) Misfit as a function of coseismic  $M_0$ . The star marks the  $M_0$  corresponding to the lowest misfit. We found the best-fitting  $M_0$  for each resampled dataset in the bootstrap, yielding a distribution of  $M_0$  estimates. (C) Test of the constrained inversion / bootstrap method using data predicted from a hypothetical slip distribution. The calculation for bounds on moment was repeated 700 times with different random errors added to the synthetic data. The fraction of times the “true” moment fell outside the bounds inferred from the constrained inversion and bootstrap is shown as a function of

confidence interval. For example, at the 95% confidence level the “true” moment should fall outside the bounds ~5% of the time.

**Figure 3:** Joint probability density function for transition depth and deep slip-rate. Murray et al. (10), used damped least squares to estimate interseismic slip-rate for a range of transition depth and deep slip-rate pairs with optimal smoothing determined by cross validation. The minimum cross validation sum of squares (CVSS), a measure of misfit, occurs at 14 km and 33 mm/yr, in keeping with independent geologic and seismic observations. We observe that CVSS is an approximately quadratic function of transition depth and deep slip-rate, suggesting that it can be used to generate a probability density function proportional to  $e^{CVSS}$ . Note the strong positive correlation between slip-rate and transition depth.

**Figure 4:** Bootstrap distributions for (A) coseismic moment, (B) interseismic moment deficit rate found using trilateration data, (C) interseismic moment deficit rate found using GPS data, and (D) predicted interevent time. 95% confidence bounds are indicated by the red lines: (A) lower bound =  $3.3 \times 10^{18}$  Nm, upper bound =  $1.0 \times 10^{19}$  Nm; (B)  $2.7 \times 10^{17}$  Nm/yr –  $7.6 \times 10^{17}$  Nm/yr; (C)  $2.2 \times 10^{17}$  Nm/yr –  $6.8 \times 10^{17}$  Nm/yr; (D) 6.7 years – 20.7 years. Green lines indicate best-fitting value using the actual (not resampled) dataset.

## References and Notes

1. Working Group on California Earthquake Probabilities, "Earthquake probabilities in the San Francisco Bay Region: 2000 to 2030 – A summary of findings" *U.S. Geol. Surv. open-file report 99-517* (1999).
2. K. Shimazaki, T. Nakata, *Geophys. Res. Lett.* **7**, 279 (1980).
3. K. Sieh et al., *Science* **260**, 171 (1993).
4. J. R. Rice, A. L. Ruina, *J. Appl. Mech. Trans. ASME* **50**, 343 (1983).
5. J. Dieterich, B. Kilgore, *Proc. Natl. Acad. Sci. U.S.A.* **93**, 3787 (1996).
6. The 1934 and 1966 Parkfield events were both preceded by  $M$  5.1 foreshocks 17 minutes before the main shock, were similar in source location and the initial stages of rupture, propagated unilaterally southeast, and had similar spatial extent of aftershocks and surface faulting. Available data for the earlier earthquakes suggest they had similar hypocenters and moment to the 1934 and 1966 events (7).
7. W. H. Bakun, T. V. McEvelly, *J. Geophys. Res.* **89**, 3051 (1984).
8. E. Roeloffs, J. Langbein, *Rev. Geophys.* **32**, 315 (1994).
9. N. E. King, P. Segall, W. Prescott, *J. Geophys. Res.* **92**, 2747 (1987).
10. J. R. Murray, P. Segall, P. Cervelli, W. Prescott, J. Svarc, *Geophys. Res. Lett.* **28**, 359 (2001).
11. R. A. Harris, P. Segall, *J. Geophys. Res.* **92**, 7945 (1987).
12. R. A. Snay, *Manuscripta Geodaetica* **14**, 391 (1989).
13. J. C. Savage, *J. Geophys. Res.* **95**, 4873 (1990).
14. P. Segall, R. Harris, *J. Geophys. Res.* **92**, 10,511 (1987).

15. The coseismic moment,  $M_o$ , is calculated from:

$$M_o = \mu \iint_A s dA$$

where  $\mu$  is the shear modulus (taken to be 30 GPa in this study),  $A$  is the area that slipped, and  $s$  is the (spatially variable) amount of slip. The moment deficit rate is

$$\dot{M}_o = \mu \iint_A (\dot{s}_\infty - \dot{s}) dA,$$

where  $\dot{s}_\infty$  is the long-term deep slip-rate and  $\dot{s}$  is the (spatially variable) forward slip-rate.

With strain as a proxy for stress, these may be used to estimate interevent time,  $t_i$ :

$$t_i = M_o / \dot{M}_o.$$

16. Trilateration (9) measures the distance between two benchmarks. The trilateration data used in the current study were collected by the California Department of Water Resources, the California Division of Mines and Geology, and the US Geological Survey (USGS), and include the data used in (11) as well as additional measurements made between 1985 and 1991. GPS (10) is used to determine the position of a single benchmark. These data were collected by the USGS. GPS data are not subject to the same errors as the trilateration data; in particular the GPS errors increase much more slowly with separation between stations. Trilateration measurements repeated over time can be used to estimate rates of distance change, while GPS measurements over time produce velocities of individual stations.

17. H. O. Johnson, D. C. Agnew, K. Hudnut, *Bull. Seismo. Soc. Am.* **84**, 660 (1994).

18. B. Efron, R. J. Tibshirani, *An Introduction to the Bootstrap* (Chapman and Hall, New York, 1993).

19. The bootstrap involves resampling the data a large number of times and repeating the inversions with each resampled dataset to result in many realizations of the estimated quantity. One can then use this distribution of estimates to obtain confidence limits on the solution inferred from the original data or sample from the distribution to get input for further calculations.
20. Measured surface offsets from the 1966 event were used to bound the estimated coseismic slip in subfaults that break the earth's surface (24). Shallow creep rates inferred using data from creepmeters, alignment arrays, and small aperture networks, were used to bound the slip-rates on these subfaults in the inversions for interseismic slip deficit rate distribution (11). For the interseismic period, the contribution to line-length rate of change or GPS velocity from slip on the creeping section of the San Andreas and from slip below the transition depth were incorporated as discussed in (10).
21. G. Wahba, *Spline Models for Observational Data* (Society for Industrial and Applied Mathematics, Philadelphia, PA, 1990).
22. P. Segall, Y. Du, *J. Geophys. Res.* **98**, 4527 (1993).
23. Y.-B. Tsai, K. Aki, *Bull. Seismo. Soc. Am.* **59**, 275 (1969).
24. S. W. Smith, M. Wyss, *Bull. Seismo. Soc. Am.* **58**, 1955 (1968).
25. Proceedings of the third conference on Tectonic Problems of the San Andreas Fault System, Stanford, CA, Sept. 6-8, 2000, G. Bokelmann, R. Kovach, eds., 179 (Stanford University Publications, Stanford, CA, 2000).

26. Noting that we had 25 years of trilateration measurements without a Parkfield earthquake, we estimate the interevent time as follows:

$$\Delta t = \frac{M_{o_{1966}}}{\dot{M}_d^t}$$

if  $M_{o_{1966}} - (\dot{M}_d^t \times 25\text{yrs}) \leq 0$ , and

$$\Delta t = 25\text{yrs} + \frac{M_{o_{1966}} - (\dot{M}_d^t \times 25\text{yrs})}{\dot{M}_d^G}$$

if  $M_{o_{1966}} - (\dot{M}_d^t \times 25\text{yrs}) > 0$ .

where the next earthquake is predicted to occur in  $1966 + \Delta t$ .  $M_{o_{1966}}$  is the coseismic moment,  $\dot{M}_d^t$  is the moment deficit rate inferred from trilateration data, and  $\dot{M}_d^G$  is that inferred from the GPS data.

27. J. Dieterich, *J. Geophys. Res.* **99**, 2601 (1994).

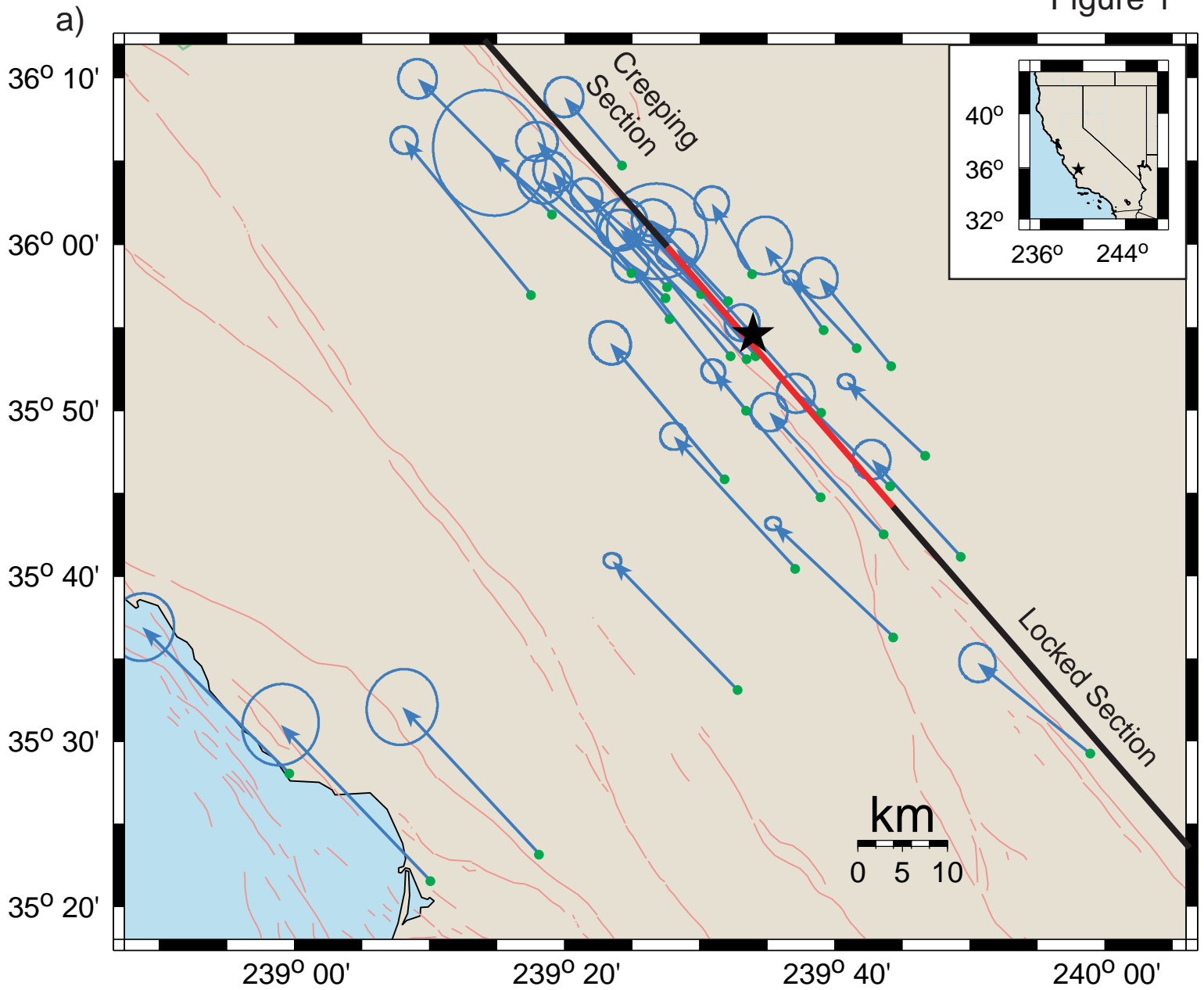
28. S. Toda, R. Stein, *J. Geophys. Res.*, in review.

29. J. B. Fletcher, P. Spudich, *J. Geophys. Res.* **103**, 835 (1998).

30. Y. Ben-Zion, J. R. Rice, R. Dmowska, *J. Geophys. Res.* **98**, 2135 (1993).

31. We thank Jim Savage for valuable commentary regarding the proper treatment of joint probability distributions, Rob Tibshirani for advice on the application of the bootstrap, John Langbein and Peter Cervelli for useful discussions of Parkfield geodesy and inversion strategies, and Will Prescott and Jerry Svarc for guidance in processing the GPS data.

Figure 1



—▶ 30 mm/yr, 95% confidence ellipse      faults

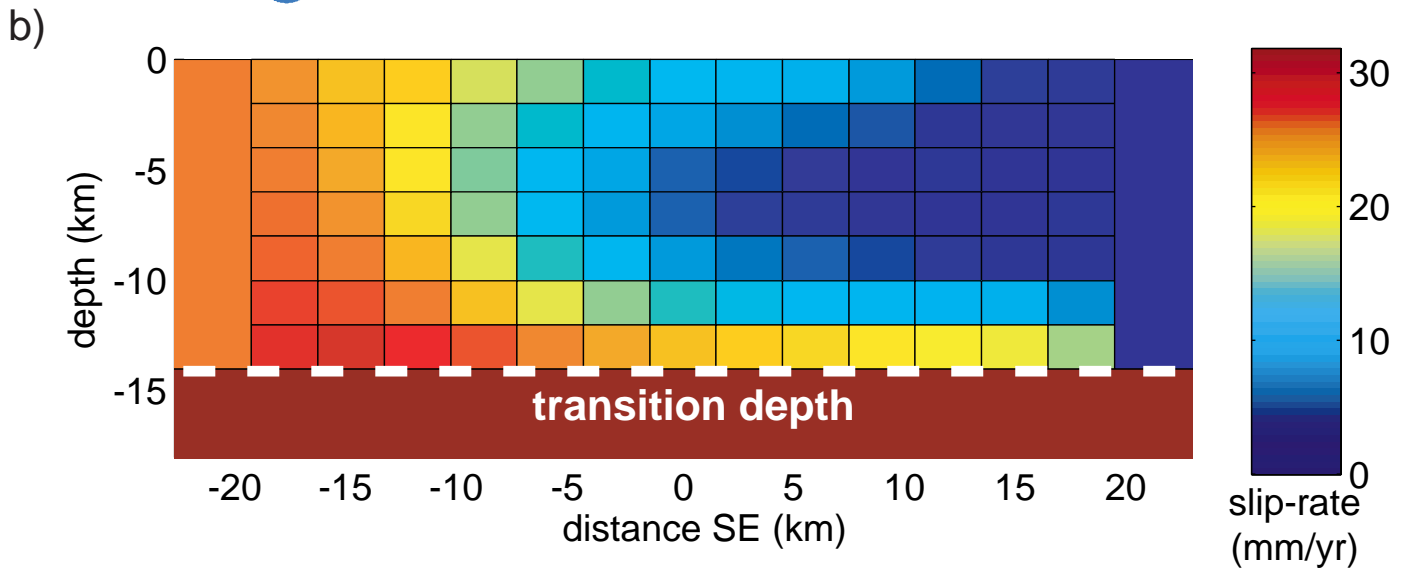


Figure 2

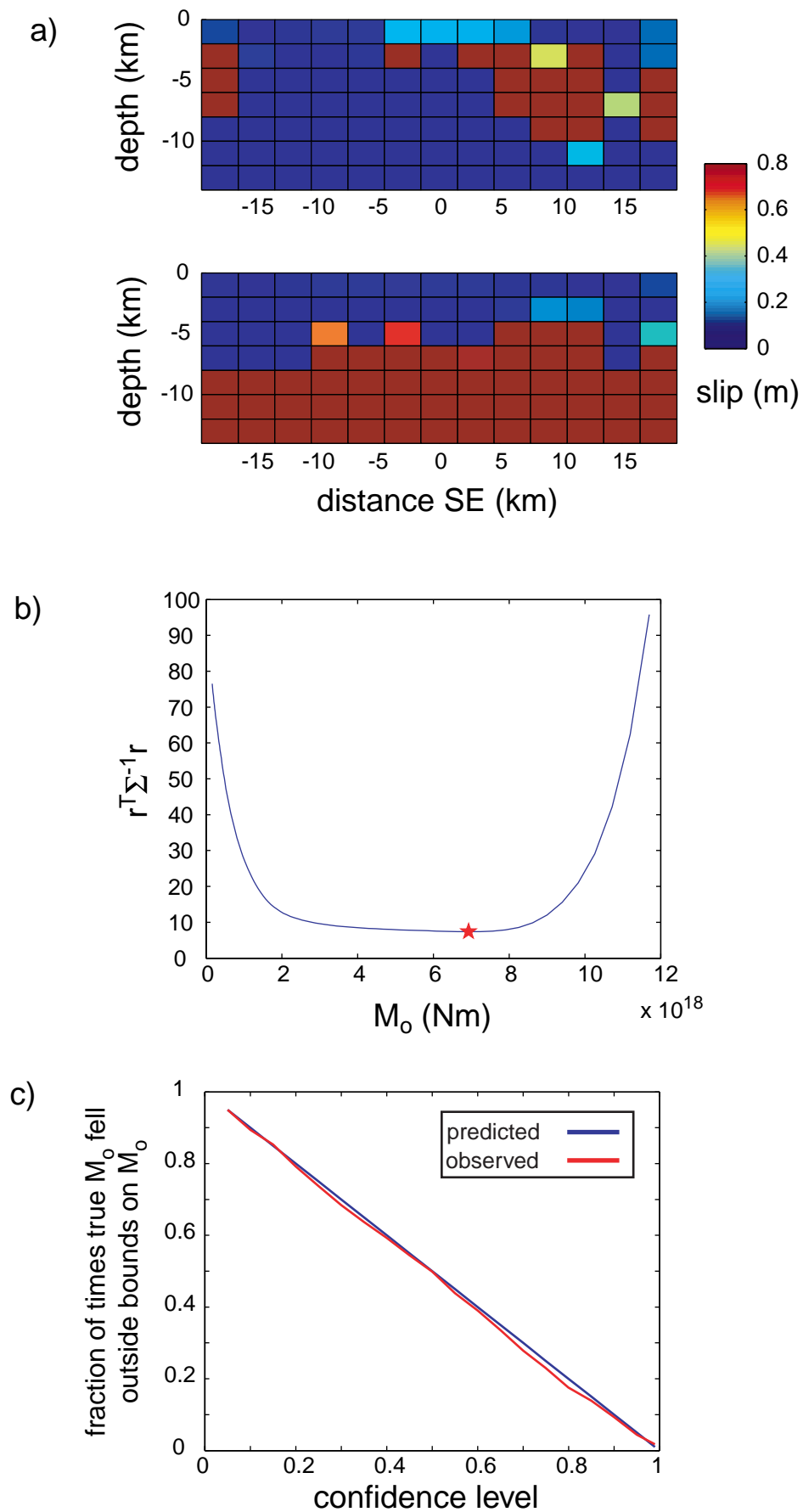


Figure 3

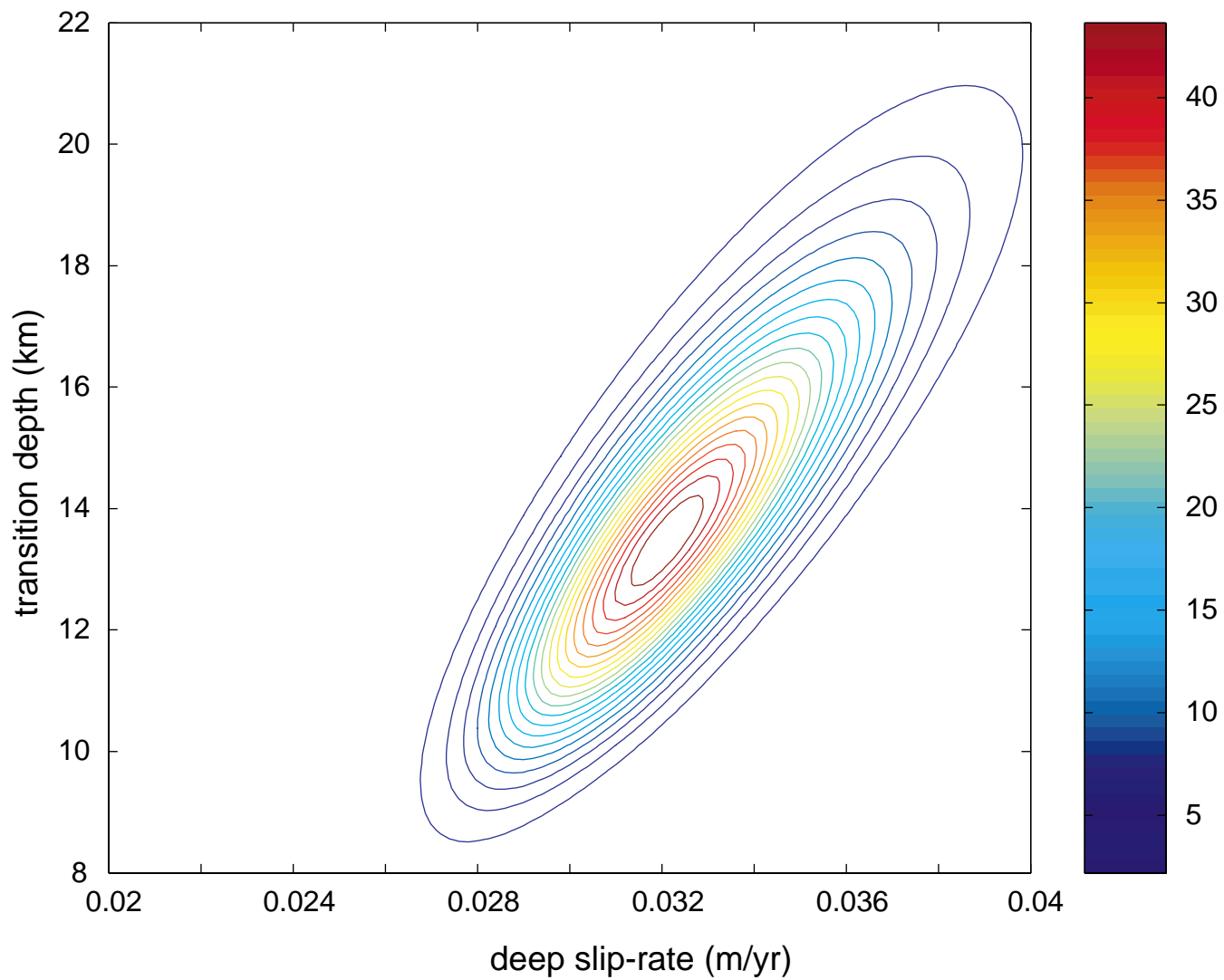


Figure 4

